Polímeros
ISSN 1678-5169 (Online)

https://doi.org/10.1590/0104-1428.20250105

ORIGINAL ARTICLE

Green fabrication of superhydrophobic poly(furfuryl alcohol)-coated melamine sponge

Thi Nhat Thang Nguyen[1]*, Huu Trung Nguyen[1], Thao Quynh Ngan Tran[1] and Xuan Thang Cao[1]*

[1]Faculty of Chemical Engineering, Industrial University of Ho Chi Minh City, Ho Chi Minh City, Vietnam
**nguyenthinhatthang@iuh.edu.vn; caoxuanthang@iuh.edu.vn*

Abstract

The increasing frequency of organic solvent pollution has raised urgent demands for efficient, sustainable, and recyclable materials for solvent-water separation. In this study, we report a green, facile strategy to fabricate a superhydrophobic melamine sponge (MS) modified with poly(furfuryl alcohol) (PFA) using a zinc-based deep eutectic solvent (DES) system. The DES, composed of choline chloride and $ZnCl_2$, served dually as both the polymerization medium and catalytic agent for the in-situ polymerization of furfuryl alcohol on the MS skeleton. The resulting PFA-coated MS (PFA/MS) retained its intrinsic porous 3D network while acquiring significantly enhanced surface roughness and hydrophobicity. Water contact angle measurements confirmed superhydrophobicity (167.6°), and the sponge exhibited high selectivity and sorption capacity toward a wide range of organic solvents. This environmentally benign, scalable approach offers a promising platform for the development of reusable sorbents in oil spill cleanup and industrial wastewater treatment.

Keywords: *deep eutectic solvent, green synthesis, poly(furfuryl alcohol), solvent-water separation, superhydrophobic sponge.*

Data Availability: All data supporting the findings of this study are available from the corresponding author upon request.

How to cite: Nguyen, T. N. T., Nguyen, H. T., Tran, T. Q. N., & Cao, X. T. (2026). Green fabrication of superhydrophobic poly(furfuryl alcohol)-coated melamine sponge. *Polímeros: Ciência e Tecnologia*, *36*(3), e20260032. https://doi.org/10.1590/0104-1428.20250105

1. Introduction

The release of petroleum-derived pollutants, industrial solvents, and organic contaminants into aquatic environments poses severe threats to both ecological systems and human health[1-4]. Oil - water mixtures resulting from accidental spills, industrial discharges, and daily operations are challenging to separate due to the immiscibility and persistence of the oil phase[5,6]. Conventional separation methods, including skimming, centrifugation, flotation, and membrane, often suffer from inefficiency, high energy consumption, or secondary pollution[7-9]. Therefore, the design of advanced sorbent materials with high selectivity, large sorption capacity, and excellent recyclability has become a crucial research direction in environmental remediation[10,11]. Among various sorbent materials, porous polymeric sponges have gained increasing attention due to their lightweight nature, high porosity, mechanical flexibility, and ease of recovery[12-15]. In particular, melamine sponge (MS), a commercially available open-cell foam, exhibits excellent structural integrity and chemical stability[16,17]. However, pristine MS is intrinsically hydrophilic, which severely limits its application in oil-water separation. To impart superhydrophobicity and oleophilicity, surface functionalization is required[18,19]. Numerous strategies have been reported for modifying MS surfaces, including physical coating, chemical grafting, carbonization, and silanization[20-26]. To date, various fabrication strategies such as dip-coating, blending, and chemical vapor deposition have been widely developed to construct superhydrophobic melamine sponges for oil/water separation. In recent years, utilizing eco-friendly, green components and biological macromolecules to achieve fluorine-free superhydrophobicity has attracted significant attention[27]. For instance, functional micro/nanoparticles like lignin microspheres, TiO_2, or MXene have been successfully assembled onto the MS skeleton to generate robust rough topologies without compromising environmental safety[28,29]. Although effective, many of these approaches often still rely on organic solvents, expensive reagents, or energy - intensive conditions, which may conflict with the principles of green chemistry. Hence, there is a pressing need for more environmentally friendly, cost-effective, and straightforward methods to develop functionalized sponges suitable for oil - water separation[30-32].

Deep eutectic solvents (DESs) have emerged as a class of green solvents with tunable properties, low toxicity, and easy preparation[33-36]. Typically formed by combining a hydrogen bond donor and acceptor, DESs can function as solvent media, reaction catalysts, and even structure-directing agents[37-40]. In particular, metal salt-based DESs such as $ZnCl_2$ - choline chloride not only provide a medium for reactions but also exhibit Lewis acid properties, making them ideal for catalyzing polymerization processes[41]. Furfuryl alcohol (FA), a bio-derived monomer from agricultural waste, can be polymerized under acidic conditions to form poly(furfuryl alcohol) (PFA), a carbon-rich polymer with hydrophobic and thermally stable properties[42,43].

By employing a DES containing $ZnCl_2$ as a catalyst, furfuryl alcohol can be polymerized in situ on MS substrates, forming a uniform PFA coating. This strategy eliminates the use of hazardous acids or organic solvents and enables one-step functionalization under mild conditions.

In this work, we propose a simple, green, and scalable route to fabricate superhydrophobic MS by coating it with PFA using a zinc-based DES system (Figure 1). The resulting PFA/MS composite maintains the original porous framework of MS while acquiring surface roughness and hydrophobicity critical for organic solvent sorption. The modified sponge exhibits strong selectivity for organic solvents, high adsorption capacity, and excellent reusability over multiple cycles. This study demonstrates the potential of DES-mediated *in-situ* polymerization as a versatile platform for developing eco-friendly sorbent materials for environmental applications.

2. Materials and Methods

2.1 Materials

MS was purchased from Gigamall shopping center, Ho Chi Minh City, Vietnam (dimensions: 10.5 × 6 × 3 cm^3). Furfuryl alcohol (FA, 98%), choline chloride (ChCl, >98%), and zinc chloride ($ZnCl_2$, >98%) were purchased from Alfa Aesar. All other solvents and reagents used were of analytical grade and employed as received. Deionized (DI) water was used throughout the experiments.

2.2 Preparation of PFA-coated melamine sponge (PFA/MS)

The $ZnCl_2$: ChCl DES was prepared as our previous work[41]. Prior to use, MS was thoroughly cleaned with a mixture of DI water and ethanol, then dried and cut into small blocks (2 × 1.5 × 1.0 cm^3). The MS blocks were immersed in a FA solution in DI water (0.2 g/mL; 10 mL total volume) and sonicated in an ultrasonic bath for 2 h to ensure deep infiltration. The pretreated MS was then transferred into a mixture of DES (0.5 g) dissolved in 8.0 mL of DI water and stirred continuously at 60 °C for 3 h to induce polymerization. After reaction, the PFA/MS samples were washed thoroughly with DI water and dried to constant weight.

2.3 Organic solvent adsorption test

The solvent adsorption capability of the PFA/MS composite was assessed using a biphasic system consisting of water and organic solvent. In a typical experiment, 200 µL of solvent was added to 100 mL of DI water in a 250 mL beaker, forming a two-phase mixture due to immiscibility. A pre-weighed sample of PFA/MS (50 mg) was gently placed into the center of the beaker without stirring. The adsorption time was recorded using a stopwatch, starting from the moment the sorbent contacted the liquid surface. The endpoint was defined as the point when the organic phase visibly disappeared or was fully absorbed into the sorbent, indicating complete uptake. This time was measured visually and averaged over at least three replicate trials for each solvent to ensure reproducibility. After adsorption, the sample was retrieved using tweezers, briefly dried on filter paper to remove excess water, and immediately weighed. The difference in mass before and after adsorption was used to calculate the amount of organic solvent absorbed. The adsorption efficiency (%) was calculated by comparing the absorbed mass to the initial mass of the added solvent.

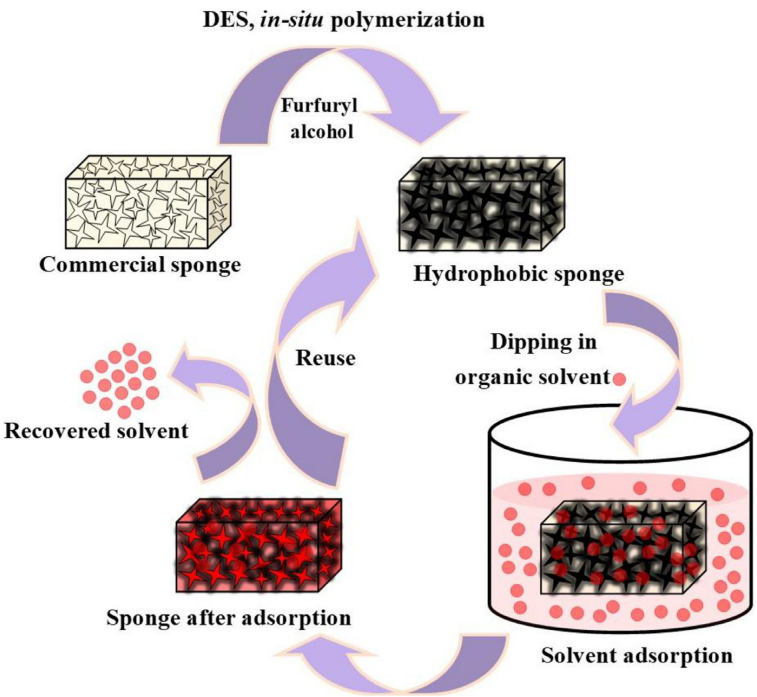

Figure 1. Synthesis of hydrophobic PFA/MS for organic solvent adsorption.

2.4 Reusability test of PFA/MS

The reusability of the PFA/MS composite was evaluated through repeated sorption–desorption cycles. In each cycle, 50 mg of PFA/MS was first used to absorb 200 µL of the target liquid in a biphasic system with 100 mL of DI water. After adsorption, the saturated sponge was removed and gently rinsed three times with 10 mL of ethanol to remove the adsorbed solvent. The cleaned PFA/MS was then dried at 40 °C in a vacuum oven prior to reusing in the next cycle. The adsorption capacity was recorded over five consecutive cycles to assess the retention of performance.

2.5 Evaluation of chemical stability and mechanical durability

The chemical stability of the superhydrophobic PFA/MS composite was evaluated by immersing the modified sponges into various corrosive media, including an acidic solution (HCl, pH 1), an alkaline solution (NaOH, pH 13), and a salt solution (NaCl, 5.0 wt%), at room temperature for 24 h. For the mechanical durability test, cyclic compression-release evaluations were performed by subjecting the composite sponge to repeated cyclic deformation strains. After the respective chemical treatments and mechanical cycles, the samples were rinsed thoroughly, completely dried at 60 °C, and their WCAs were re-measured.

3. Results and Discussions

The stepwise transformation of the PFA/MS composite is illustrated in Figure 2. Initially, MS was added into a mixture of FA and DES. Upon stirring, the mixture gradually turned light yellow, indicating the onset of FA polymerization and its partial interaction with the sponge framework (Figure 2a). After polymerization and thorough washing, the modified sponge was dried to yield a dark brown porous monolith (Figure 2b). Figure 2c visually demonstrates the water-repellent character of the modified sponge, where a water droplet rests on the surface without spreading suggesting a transition to a hydrophobic state. To complement this, the precise wettability was quantified via an optical contact angle meter, revealing an exceptional water contact angle (WCA) of 167.6° (Figure 2d). This exceptional water repellency can be attributed to the micro-/mesoporous structure formed during the polymerization and drying process, combined with the low surface energy of the crosslinked furanic matrix. The strong repulsion toward water enables efficient phase separation and facilitates rapid adsorption of organic contaminants, further reinforcing the potential application of PFA/MS materials in solvent cleanup and environmental remediation. The surface morphologies of the pristine MS and PFA/MS were examined using SEM.

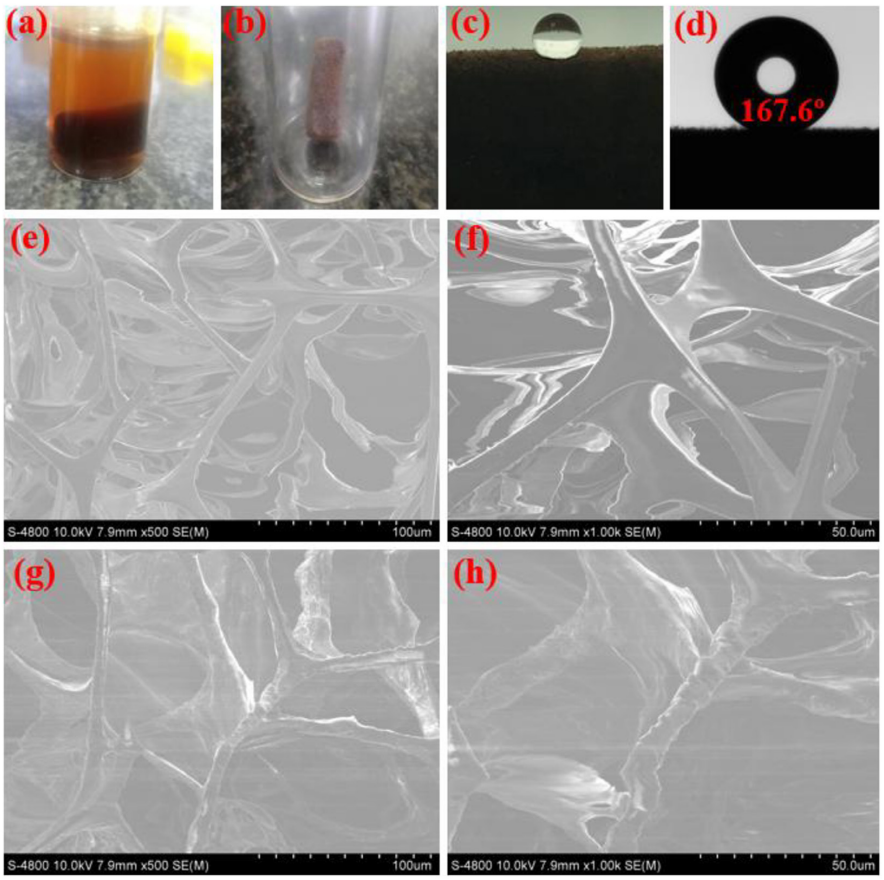

Figure 2. Photographs and morphological characterizations: (a) MS immersed in DES/FA mixture; (b) PFA/MS composite after polymerization; (c) digital photograph of water droplet on PFA/MS surface; (d) optical WCA image of PFA/MS; SEM images of pristine MS at (e) 500× and (f) 1000× magnifications, and PFA/MS at (g) 500× and (h) 1000× magnifications.

As shown in Figure 2e and f, the unmodified MS exhibits a typical three-dimensional open-cell network structure composed of interconnected, smooth struts forming a highly porous skeleton. The surface of the MS framework appears clean and uniform, with well-defined edges and sharp pore boundaries, consistent with its commercial fabrication. Upon surface modification with PFA, notable changes in surface characteristics were observed, while the overall 3D porous architecture was retained (Figure 2g and h). The PFA coating results in increased surface roughness and a visible loss of sharpness in the skeletal framework, indicating the formation of a continuous polymer layer over the melamine backbones. The once-smooth surfaces become irregular and textured, suggesting successful deposition and *in-situ* polymerization of FA throughout the skeleton. This roughened morphology is advantageous for enhancing surface energy and hydrophobic interactions, which is desirable for subsequent organic solvent adsorption. Furthermore, the uniform coverage of PFA across the sponge matrix implies effective penetration and catalytic polymerization throughout the DES-mediated process. These morphological features confirm that the DES-mediated polymerization proceeded effectively throughout the sponge matrix while maintaining the essential macroporous structure critical for capillary-driven adsorption and separation performance.

The FTIR spectrum of pristine MS reveals characteristic vibrational bands associated with its triazine-based polymeric structure (Figure 3a). Prominent peaks at 1556, 848, and 796 cm^{-1} are attributed to C=N stretching and ring breathing modes of the melamine backbone. A broad band centered at 1679 cm^{-1} is assigned to N–H bending vibrations, potentially coupled with conjugated C=N stretching. Notably, the appearance of a peak at 1749 cm^{-1} suggests the presence of residual carbonyl-containing groups, likely originating from processing additives of melamine-formaldehyde resins. Additionally, the high-frequency bands at 3739 and 3624 cm^{-1} may arise from N–H stretching or adsorbed moisture. These features indicate that the commercial MS sample contains both intrinsic melamine functionalities and minor polymeric additives from its manufacturing process. The FTIR spectrum of pure PFA, a broad absorption band around 3400 cm^{-1} corresponds to O–H stretching vibrations from residual hydroxyl groups or intra-/intermolecular hydrogen bonding, which may result from incomplete polymerization or moisture uptake. A distinct peak at 3118 cm^{-1} is assigned to =C–H stretching of the furan ring, confirming the aromatic-like character of the polymer backbone.

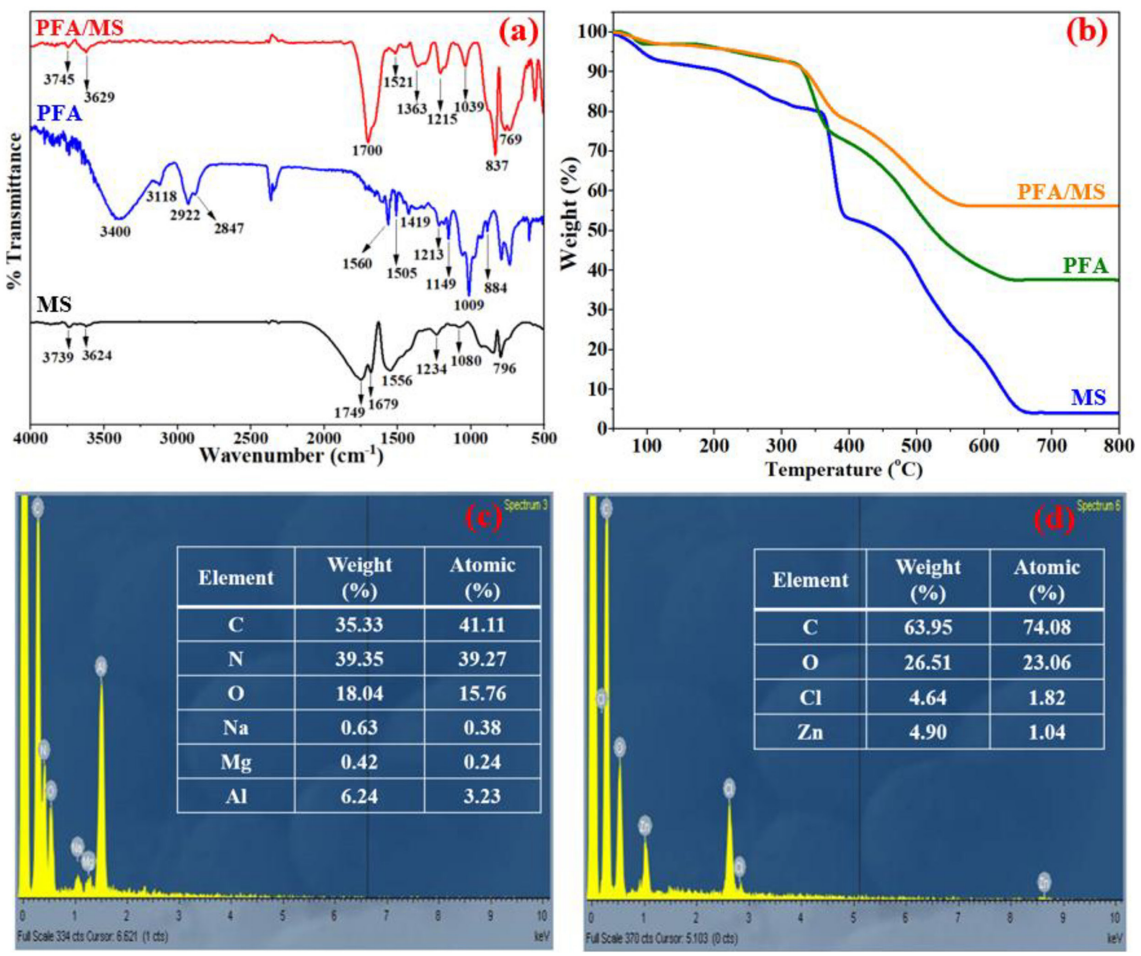

Figure 3. Characterization of pristine MS, PFA, and PFA/MS composite: (a) FTIR spectra; (b) TGA curves; EDX spectra and elemental compositions of (c) MS and (d) PFA/MS.

Aliphatic C–H stretching vibrations of methylene and methyl groups are observed at 2922 and 2847 cm^{-1}, respectively. In the fingerprint region, strong bands at 1560 and 1505 cm^{-1} are indicative of C=C stretching and ring vibration modes of the furan unit, while the peak at 1419 cm^{-1} corresponds to C–H in-plane deformation. The absorptions at 1213 and 1149 cm^{-1} are attributed to asymmetric C–O–C stretching, suggesting the formation of ether linkages during acid-catalyzed polymerization. A well-resolved band at 1009 cm^{-1} represents C–O stretching of alcohol or ether groups. The presence of a peak at 884 cm^{-1}, assigned to out-of-plane =C–H bending of the furan ring, further confirms the preservation of furanic moieties in the polymer. These results are in good agreement with previously reported spectra, validating the successful formation of PFA. The FTIR spectrum of PFA/MS exhibits combined features from both the MS substrate and the PFA coating, confirming successful surface modification. The absorption band in the high-frequency region (~3745 and 3629 cm^{-1}) arises from overlapping O–H and N–H stretching vibrations, indicative of hydrogen bonding and contributions from both components. The appearance of a medium-intensity peak at 1700 cm^{-1} may be associated with residual C=O stretching, possibly due to slight oxidation or unreacted functional groups on the surface. The peak at 1521 cm^{-1} reflects a convolution of C=C stretching from the furan rings and deformation vibrations of the triazine ring in MS, providing evidence of the chemical hybridization. A band at 1363 cm^{-1} corresponds to overlapping C–H and C–N bending modes. Characteristic PFA-derived bands at 1215 and 1039 cm^{-1} are attributed to asymmetric C–O–C stretching vibrations, confirming the formation of ether linkages. Finally, peaks at 837 and 769 cm^{-1} can be ascribed to out-of-plane bending vibrations of both the triazine and furan rings. Collectively, the FTIR data confirm the successful in-situ polymerization of FA on the MS framework, resulting in PFA/MS composite material that integrates the structural characteristics of MS with the surface chemistry of PFA-critical for the enhanced hydrophobic and oleophilic performance in organic solvent–water separation applications. The thermal stability of the materials was further evaluated by TGA, as illustrated in Figure 3b. The pristine MS exhibited a continuous weight loss starting from around 100 °C, which is mainly attributed to the evaporation of adsorbed moisture and the progressive degradation of organic components. A sharp decomposition step occurred between 300–500 °C, leading to a residual weight of less than 5%, indicating the presence of significant thermolabile components. In contrast, pure PFA demonstrated markedly enhanced thermal stability, with the main weight loss occurring between 350–600 °C and a final residue of approximately 40%. This two-stage degradation pattern corresponds to the thermal decomposition of cross-linked PFA chains and the charring of carbonaceous structures. Notably, the PFA/MS composite exhibited intermediate thermal behavior. Its onset of degradation was slightly delayed compared to MS, beginning around 200 °C, and showed a more gradual weight loss profile. The final residue of ~55% suggests that the incorporation of MS enhances the thermal resistance of PFA, likely due to the formation of a more stable hybrid structure and possible barrier effects exerted by the MS framework. Overall, the TGA results confirm that the integration of MS into the PFA matrix significantly improves its thermal stability, making the composite more suitable for high-temperature applications.

The elemental compositions of pristine MS and PFA/MS composite were analyzed using EDX spectroscopy, as presented in Figure 3c and d. The spectrum of pristine MS (Figure 3c) revealed a high content of nitrogen (39.35 wt%) and carbon (35.33 wt%), consistent with the triazine-rich melamine structure. Oxygen was also detected at 18.04 wt%, possibly due to surface-bound hydroxyl or carbonyl functionalities. Interestingly, a significant amount of aluminum (6.24 wt%) was identified, along with detectable levels of magnesium and sodium. These additional elements are likely residues from commercial additives such as inorganic flame retardants or catalysts incorporated during the fabrication of the raw melamine sponge. In contrast, the EDX spectrum of the PFA/MS composite (Figure 3d) showed a marked increase in carbon content (63.95 wt%) accompanied by a sharp decrease in nitrogen and oxygen levels. The nitrogen signal, characteristic of melamine, was nearly absent—likely due to the complete encapsulation of the MS skeleton by the nitrogen-free PFA layer. Furthermore, aluminum and magnesium peaks disappeared, suggesting that these elements were either washed away during the polymerization and post-treatment steps or became undetectable beneath the uniform polymer coating. The presence of chlorine (4.64 wt%) and zinc (4.90 wt%) in the composite indicates residual components from the choline chloride–$ZnCl_2$ DES used during in-situ polymerization. Altogether, these compositional changes confirm the successful modification of MS by PFA and the incorporation of DES-derived elements into the final structure.

To further confirm the chemical states and surface functionalities before and after modification, XPS analysis was performed on both pristine MS and PFA/MS composite. Although nitrogen was not detected in the EDX spectra of PFA/MS due to its surface sensitivity limitations, XPS analysis confirms the presence of nitrogen-containing species (C=N) in the near-surface region. As shown in Figure 4a and 4d, the N 1s spectra of both pristine MS and PFA/MS exhibit a dominant peak centered at approximately 398.5 eV, which is attributed to the C=N bonds in the triazine rings of melamine. The deconvoluted C 1s spectrum of PFA/MS (Figure 4b) reveals three distinct components located at ~284.6, 286.0, and 288.2 eV, corresponding to C–C/C–H, C–N, and C–O species, respectively. The appearance of the C–O signal confirms the successful incorporation of oxygenated functional groups derived from the PFA network. The O 1s spectrum of PFA/MS (Figure 4c) displays a broad peak centered at ~532.5 eV, which is assigned to C–O–C bonds. This further supports the presence of ether functionalities introduced by the PFA coating. Taken together, these XPS results validate the successful surface modification of MS with PFA, which contributes to enhanced surface hydrophobicity and chemical functionality.

To better evaluate the performance of PFA/MS, its WCA was compared with those of various modified sponge materials reported in the literature (Table S1, Supplementary Material). These reference materials employ a wide range of surface modifiers, including fluorinated silanes, long-chain alkyl groups, and hydrophobic polymers such as polydimethylsiloxane (PDMS), often combined with nanomaterials like Fe_3O_4, Ag, graphene oxide (GO), or carbon nanotubes (CNTs).

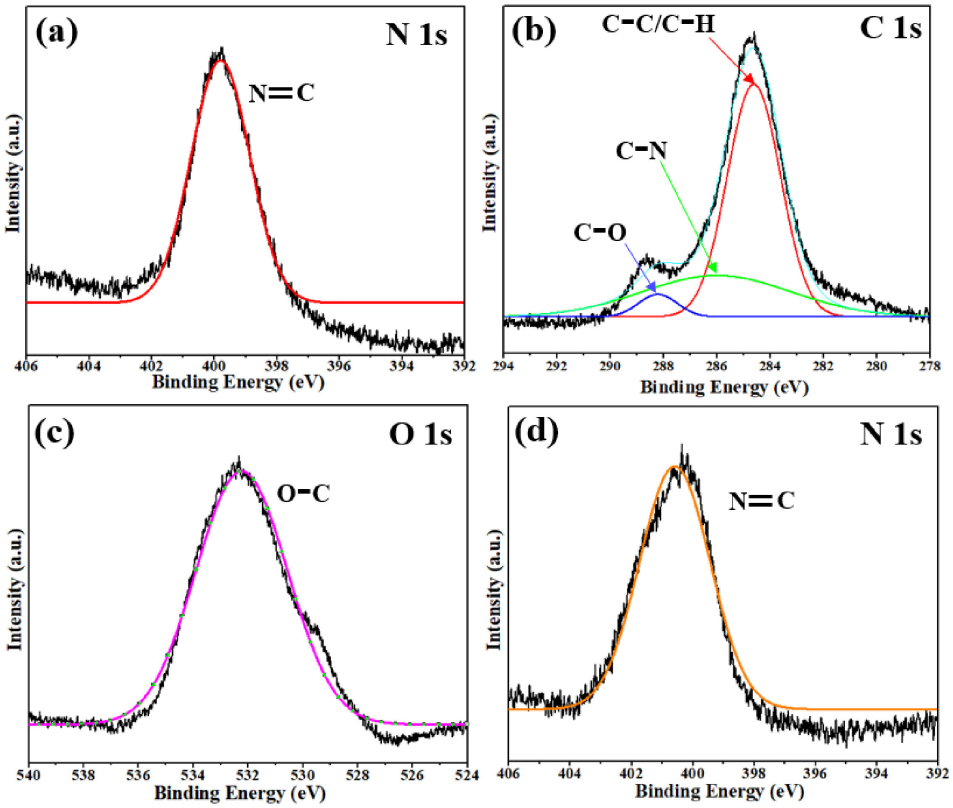

Figure 4. High-resolution XPS core-level spectra of (a) pristine MS and (b) C 1s, (c) O 1s, and (d) N 1s regions of PFA/MS composite.

These combinations enhance surface roughness and reduce surface energy, leading to high WCAs in the range of 150–170°. In comparison, the PFA/MS fabricated in this work demonstrates a superior WCA of 167.6°, which is among the highest reported values. Importantly, this high hydrophobicity was achieved through an eco-friendly, fluorine-free method using DES-induced in situ polymerization of FA. Unlike many prior studies that rely on complex multistep synthesis or the use of environmentally harmful reagents, our approach provides a simple, scalable, and green alternative without compromising performance. This highlights the potential of DES-based surface engineering as a sustainable platform for developing next-generation superhydrophobic materials.

The solvent separation performance of the composite was assessed against a range of organic solvents, as shown in Figure 5. The PFA/MS composite exhibited variable separation efficiencies toward different organic solvents, ranging from 71.2% to 98.6%. The highest efficiency was observed for toluene (98.6%) and petroleum ether (95.8%), followed by ethyl acetate (90.4%) and tetrahydrofuran (89.3%). Lower efficiencies were recorded for n-hexane (76.0%), chloroform (73.1%), and dichloromethane (71.2%). These differences can be attributed to the physicochemical properties of the solvents, particularly their polarity, density, and molecular interaction with the PFA/MS surface. Non-polar or low-polarity solvents such as toluene and petroleum ether exhibited stronger affinity with the hydrophobic and oleophilic surface of the sponge, facilitating capillary-driven adsorption. In contrast, dense solvents like chloroform

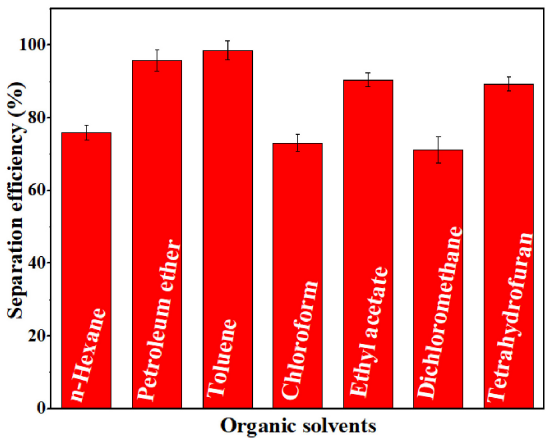

Figure 5. Separation efficiency of the PFA/MS for different organic solvents. The values represent the average of at least three measurements.

and dichloromethane may rapidly flow through the porous matrix, reducing contact time and thus lowering retention. Ethyl acetate and tetrahydrofuran, as moderately polar solvents, displayed intermediate uptake behavior due to balanced interactions with the sponge surface. Although the overall separation efficiencies were lower than some previously reported superabsorbent materials, it is worth noting that the current system emphasizes green synthesis

and durability over multiple cycles, with no need for post-surface modification. Further optimization of the sponge porosity and surface energy could improve the uptake of heavier or polar solvents.

The recyclability of the PFA/MS composite was assessed through five consecutive sorption–desorption cycles using petroleum ether and ethyl acetate as representative test liquids. As shown in Figure 6, the adsorption capacity gradually declined with each cycle. For petroleum ether, the efficiency decreased from 95.8% in the first cycle to 74.6% after five cycles, while ethyl acetate showed a reduction from 90.4% to 70.3% over the same period. This decline in performance may be attributed to partial blockage of pores or incomplete desorption of residual solvent after each regeneration step. Although ethanol washing effectively removed most of the absorbed liquids, trace residues likely remained within the porous structure, reducing available active sites. Additionally, mechanical handling during repeated drying and rinsing might have slightly altered sponge morphology or surface functionality. Nevertheless, the material retained over 70% capacity after five cycles, indicating moderate recyclability. These results confirm that PFA/MS is not only effective for one-time separation, but also viable for multiple uses in practical applications such as solvent recovery and oil–water remediation.

For practical oil/water separation, sorbent materials must withstand harsh chemical environments and repeated physical deformations during oil recovery cycles. Therefore, the stability and durability of the PFA/MS composite were systematically investigated. As shown by the experimental results, the PFA/MS composite successfully retained its superhydrophobicity, exhibiting WCAs consistently greater than 150° after 24 h of exposure to strong acid (pH 1), strong base (pH 13), and hypersaline (5.0 wt% NaCl) solutions. Furthermore, the composite demonstrated reliable mechanical durability, maintaining its stable porous framework and surface superhydrophobicity without structural collapse or peeling of the coating after cyclic compression tests (data not shown). This excellent combined stability is in strong agreement with recently reported fluorine-free functionalized MS[28,29], where robust protective polymeric networks effectively reinforce the underlying sponge skeleton.

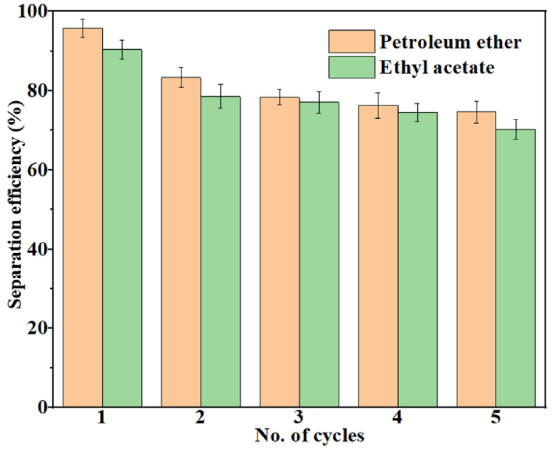

Figure 6. Reusability of the PFA/MS composite over five sorption–desorption cycles.

Due to the inherent chemical inertness, high stability, and robust interfacial adhesion of the cross-linked PFA coating, the surface chemistry and rough topology remain stable against chemical erosion and mechanical stress, ensuring dependable separation performance over long-term usage.

4. Conclusions

In this study, a PFA/MS was successfully fabricated through a DES-assisted polymerization strategy. The resulting material exhibited a remarkably high WCA of 167.6°, placing it in the category of superhydrophobic materials and highlighting the potential of this green and fluorine-free approach for scalable surface engineering. Comprehensive physicochemical characterizations confirmed the structural and chemical integration of PFA onto the melamine sponge. FTIR spectra revealed characteristic peaks of triazine and furan rings, indicating the coexistence of MS and PFA networks. TGA showed enhanced thermal stability, with a residual mass of ~55% at 800 °C, supporting the thermal robustness of the composite. EDX analysis confirmed increased carbon content after modification, further evidence that PFA coating is successful. Importantly, XPS analysis provided insights into surface chemical states. The presence of C=N peaks in the N 1s region and the emergence of C–O functionalities in the C 1s and O 1s spectra confirmed the successful introduction of oxygenated groups from the PFA network. These findings validate the chemical modification of the sponge surface, which plays a crucial role in tuning hydrophobicity and interfacial properties. Functionally, the PFA/MS composite demonstrated rapid and selective adsorption of various organic solvents, with high efficiency for toluene (98.6%), petroleum ether (95.8%), and ethyl acetate (90.4%). The material also showed good reusability, retaining over 70% of its original adsorption capacity after five cycles for both petroleum ether and ethyl acetate. Overall, the PFA/MS composite offers a low-cost, durable, and environmentally friendly platform for hydrophobic contaminant separation. Its facile synthesis, robust physicochemical properties, and excellent separation performance highlight its potential for practical applications in industrial wastewater treatment and environmental cleanup technologies.

5. Author's Contribution

- **Conceptualization** – Thi Nhat Thang Nguyen; Xuan Thang Cao.
- **Data curation** – Huu Trung Nguyen; Thao Quynh Ngan Tran.
- **Formal analysis** – Thi Nhat Thang Nguyen; Huu Trung Nguyen.
- **Funding acquisition** – Xuan Thang Cao.
- **Investigation** – Thi Nhat Thang Nguyen; Thao Quynh Ngan Tran.
- **Methodology** – Thi Nhat Thang Nguyen; Xuan Thang Cao.
- **Project administration** – Xuan Thang Cao.
- **Resources** – Thao Quynh Ngan Tran.
- **Software** – NA.

- **Supervision** – Xuan Thang Cao.
- **Validation** – Huu Trung Nguyen.
- **Visualization** – Thao Quynh Ngan Tran.
- **Writing – original draft** – Thi Nhat Thang Nguyen.
- **Writing – review & editing** – Xuan Thang Cao; Huu Trung Nguyen; Thao Quynh Ngan Tran.

6. Acknowledgements

The authors would like to thank the Industrial University of Ho Chi Minh City for general support and encouragement during this research.

7. References

1. Pereira, L. C., Souza, A. O., Bernardes, M. F. F., Pazin, M., Tasso, M. J., Pereira, P. H., & Dorta, D. J. (2015). A perspective on the potential risks of emerging contaminants to human and environmental health. *Environmental Science and Pollution Research International*, *22*(18), 13800-13823. https://doi.org/10.1007/s11356-015-4896-6. PMid:26201652.
2. Jan, S., Mishra, A. K., Bhat, M. A., Bhat, M. A., & Jan, A. T. (2023). Pollutants in aquatic systems: a frontier perspective of emerging threat and strategies to solve the crisis for safe drinking water. *Environmental Science and Pollution Research International*, *30*(53), 113242-113279. https://doi.org/10.1007/s11356-023-30302-4. PMid:37864686.
3. Duarte, H., Aliaño-González, M. J., Romano, A., & Medronho, B. (2024). Advancements in detection and mitigation strategies for petroleum-derived contaminants in aquatic environments: a comprehensive review. *Sensors (Basel)*, *24*(11), 3284. https://doi.org/10.3390/s24113284. PMid:38894076.
4. Du, Y., Xu, X., Liu, Q., Bai, L., Hang, K., & Wang, D. (2022). Identification of organic pollutants with potential ecological and health risks in aquatic environments: progress and challenges. *The Science of the Total Environment*, *806*(Part 3), 150691. https://doi.org/10.1016/j.scitotenv.2021.150691. PMid:34600995.
5. Tian, Y., Zhou, J., He, C., He, L., Li, X., & Sui, H. (2022). The formation, stabilization and separation of oil–water emulsions: A review. *Processes (Basel, Switzerland)*, *10*(4), 738. https://doi.org/10.3390/pr10040738.
6. Gohil, J. M., Kwon, G., Bhunia, P., Dutta, K., & Boukherroub, R. (2022). *Overview on oil/water separation techniques and working principles*. In R. Boukherroub, K. Dutta & J. Gohil (Eds.), *Oil–water mixtures and emulsions: membrane materials for separation and treatment* (Vol. *1*, pp. 247-304). Washington, DC: American Chemical Society. https://doi.org/10.1021/bk-2022-1407.ch007
7. Rubio, J., Souza, M. L., & Smith, R. W. (2002). Overview of flotation as a wastewater treatment technique. *Minerals Engineering*, *15*(3), 139-155. https://doi.org/10.1016/S0892-6875(01)00216-3.
8. Liu, B., Chen, B., Ling, J., Matchinski, E. J., Dong, G., Ye, X., Wu, F., Shen, W., Liu, L., Lee, K., Isaacman, L., Potter, S., Hynes, B., & Zhang, B. (2022). Development of advanced oil/water separation technologies to enhance the effectiveness of mechanical oil recovery operations at sea: potential and challenges. *Journal of Hazardous Materials*, *437*, 129340. https://doi.org/10.1016/j.jhazmat.2022.129340. PMid:35728323.
9. Li, B., Qi, B., Guo, Z., Wang, D., & Jiao, T. (2023). Recent developments in the application of membrane separation technology and its challenges in oil–water separation: A review. *Chemosphere*, *327*, 138528. https://doi.org/10.1016/j.chemosphere.2023.138528. PMid:36990363.
10. Ma, Q., Cheng, H., Fane, A. G., Wang, R., & Zhang, H. (2016). Recent development of advanced materials with special wettability for selective oil/water separation. *Small*, *12*(16), 2186-2202. https://doi.org/10.1002/smll.201503685. PMid:27000640.
11. Odoom, J., Iorhemen, O. T., & Li, J. (2025). Advances in adsorption for oily wastewater treatment: eco-friendly adsorbents and analytical insights. *Energy, Ecology & Environment*, *10*(1), 15-44. https://doi.org/10.1007/s40974-024-00332-w.
12. Wang, Z., Ma, H., Chu, B., & Hsiao, B. S. (2017). Super-hydrophobic modification of porous natural polymer "luffa sponge" for oil absorption. *Polymer*, *126*, 470-476. https://doi.org/10.1016/j.polymer.2017.05.068.
13. Koroleva, M. Y., Shirokikh, S. A., Khasanova, L. K., Babusenko, E. S., & Yurtov, E. V. (2019). Highly porous polymeric sponges for oil sorption. *Mendeleev Communications*, *29*(2), 176-177. https://doi.org/10.1016/j.mencom.2019.03.020.
14. Gupta, S., & Tai, N.-H. (2016). Carbon materials as oil sorbents: A review on the synthesis and performance. *Journal of Materials Chemistry. A, Materials for Energy and Sustainability*, *4*(5), 1550-1565. https://doi.org/10.1039/C5TA08321D.
15. Fouladi, M., Heidari, M. K., & Tavakoli, O. (2023). Development of porous biodegradable sorbents for oil/water separation: A critical review. *Journal of Porous Materials*, *30*(3), 1037-1053. https://doi.org/10.1007/s10934-022-01385-0.
16. Shi, Y., Liu, G., Jin, R., Xu, H., Wang, Q., & Gao, S. (2019). Carbon materials from melamine sponges for supercapacitors and lithium battery electrode materials: A review. *Carbon Energy*, *1*(2), 253-275. https://doi.org/10.1002/cey2.19.
17. Feng, Y., & Yao, J. (2018). Design of melamine sponge-based three-dimensional porous materials toward applications. *Industrial & Engineering Chemistry Research*, *57*(22), 7322-7330. https://doi.org/10.1021/acs.iecr.8b01232.
18. He, L., Qi, X., He, J., Li, C., Wei, W., Zhang, X., & Gao, Z. (2024). Research progress in hydrophobic modification of melamine sponge and its application in oil–water separation field. *Journal of Environmental Chemical Engineering*, *12*(3), 112536. https://doi.org/10.1016/j.jece.2024.112536.
19. Zhou, X., Li, D., Wang, L., Wang, Q., Wang, Z., Jing, Q., Marisol, R., & Li, L. (2025). Recent advances in the modification of melamine sponge for oil–water separation. *Journal of Materials Science and Technology*, *207*, 209-224. https://doi.org/10.1016/j.jmst.2024.04.013.
20. Dong, H., Zhan, Y., Sun, A., Chen, Y., & Chen, X. (2023). Magnetically responsive and durable super-hydrophobic melamine sponge material. *Colloids and Surfaces. A, Physicochemical and Engineering Aspects*, *662*, 130933. https://doi.org/10.1016/j.colsurfa.2023.130933.
21. Hojatjalali, M., Bahraminia, S., & Anbia, M. (2025). Superhydrophobic magnetic melamine sponge modified by flowerlike ZnO and stearic acid using dip coating method for oil and water separation. *Scientific Reports*, *15*(1), 7378. https://doi.org/10.1038/s41598-025-92246-8. PMid:40025248.
22. Zhang, T., Han, L., Yang, G., Schubert, D. W., & Duan, C. (2025). Optimizing melamine sponges modified with titanium dioxide nanoparticles for environmental and industrial applications. *Journal of Applied Polymer Science*, *142*(13), e56661. https://doi.org/10.1002/app.56661.
23. Stolz, A., Le Floch, S., Reinert, L., Ramos, S. M. M., Tuaillon-Combes, J., Soneda, Y., Chaudet, P., Baillis, D., Blanchard, N., Duclaux, L., & San-Miguel, A. (2016). Melamine-derived carbon sponges for oil–water separation. *Carbon*, *107*, 198-208. https://doi.org/10.1016/j.carbon.2016.05.059.
24. Lei, Z., Zhang, G., Deng, Y., & Wang, C. (2017). Thermoresponsive melamine sponges with switchable wettability by interface-initiated atom transfer radical polymerization for oil/water separation. *ACS Applied Materials & Interfaces*, *9*(10), 8967-8974. https://doi.org/10.1021/acsami.6b14565. PMid:28229584.

25. Sun, Y., Wang, W.-R., Li, D.-Y., Xu, S.-Y., Lin, L., Lu, M.-L., Fan, K., Xing, C.-Y., Li, L.-F., & Li, J.-H. (2024). Superhydrophobic melamine sponge prepared by radiation-induced grafting technology for efficient oil–water separation. *Nuclear Science and Techniques*, *35*(9), 147. https://doi.org/10.1007/s41365-024-01507-0.
26. Pham, V. H., & Dickerson, J. H. (2014). Superhydrophobic silanized melamine sponges as high-efficiency oil absorbent materials. *ACS Applied Materials & Interfaces*, *6*(16), 14181-14188. https://doi.org/10.1021/am503503m. PMid:25039789.
27. He, Z., Wang, M., & Ma, S. (2024). Porous lignin-based composites for oil/water separation: A review. *International Journal of Biological Macromolecules*, *260*(Pt 2), 129569. https://doi.org/10.1016/j.ijbiomac.2024.129569. PMid:38253151.
28. Qiao, L., Zhou, Z., Wang, M., & He, Z. (2025). Lignin Microsphere/TiO_2 Composite-Based Melamine Sponge with Superhydrophobic and Photothermal Properties for Oil/Water Separation and Anti-Icing. *Langmuir : The ACS Journal of Surfaces and Colloids*, *41*(21), 13233-13248. https://doi.org/10.1021/acs.langmuir.5c00913. PMid:40397029.
29. Wang, M., Qiao, L., Ma, S., & He, Z. (2024). Facile Preparation of photothermal superhydrophobic melamine sponge decorated with Mxene and Lignin Particles for efficient oil/water separation, fast crude oil recovery, and active deicing. *Langmuir : The ACS Journal of Surfaces and Colloids*, *40*(11), 5978-5991. https://doi.org/10.1021/acs.langmuir.3c04006. PMid:38443344.
30. Peng, M., Zhu, Y., Li, H., He, K., Zeng, G., Chen, A., Huang, Z., Huang, T., Yuan, L., & Chen, G. (2019). Synthesis and application of modified commercial sponges for oil–water separation. *Chemical Engineering Journal*, *373*, 213-226. https://doi.org/10.1016/j.cej.2019.05.013.
31. Farrokhi, S. J., Pakzad, H., Fakhri, M., & Moosavi, A. (2021). Superhydrophobic home-made polyurethane sponges for versatile and cost-effective oil and water separation. *Separation and Purification Technology*, *276*, 119240. https://doi.org/10.1016/j.seppur.2021.119240.
32. Sam, E. K., Liu, J., & Lv, X. (2021). Surface engineering materials of superhydrophobic sponges for oil/water separation: A review. *Industrial & Engineering Chemistry Research*, *60*(6), 2353-2364. https://doi.org/10.1021/acs.iecr.0c05906.
33. Hessel, V., Tran, N. N., Razi Asrami, M., Tran, Q. D., Long, N. V. D., Escribà-Gelonch, M., Osorio Tejada, J., Linke, S., & Sundmacher, K. (2022). Sustainability of green solvents: review and perspective. *Green Chemistry*, *24*(2), 410-437. https://doi.org/10.1039/D1GC03662A.
34. Liu, J., Li, X., & Row, K. H. (2022). Development of deep eutectic solvents for sustainable chemistry. *Journal of Molecular Liquids*, *362*, 119654. https://doi.org/10.1016/j.molliq.2022.119654.
35. Mushtaq, M., Butt, F. W., Akram, S., Ashraf, R., & Ahmed, D. (2024). Deep eutectic liquids as tailorable extraction solvents: a review of opportunities and challenges. *Critical Reviews in Analytical Chemistry*, *54*(6), 1634-1660. https://doi.org/10.1080/10408347.2022.2125284. PMid:36148704.
36. Prabhune, A., & Dey, R. (2023). Green and sustainable solvents of the future: deep eutectic solvents. *Journal of Molecular Liquids*, *379*, 121676. https://doi.org/10.1016/j.molliq.2023.121676.
37. Abo-Hamad, A., Hayyan, M., AlSaadi, M. A., & Hashim, M. A. (2015). Potential applications of deep eutectic solvents in nanotechnology. *Chemical Engineering Journal*, *273*, 551-567. https://doi.org/10.1016/j.cej.2015.03.091.
38. Khandelwal, S., Tailor, Y. K., & Kumar, M. (2016). Deep eutectic solvents (DESs) as eco-friendly and sustainable solvent/catalyst systems in organic transformations. *Journal of Molecular Liquids*, *215*, 345-386. https://doi.org/10.1016/j.molliq.2015.12.015.
39. Liu, P., Hao, J.-W., Mo, L.-P., & Zhang, Z.-H. (2015). Recent advances in the application of deep eutectic solvents as sustainable media as well as catalysts in organic reactions. *RSC Advances*, *5*(60), 48675-48704. https://doi.org/10.1039/C5RA05746A.
40. Gutiérrez, M. C., Carriazo, D., Ania, C. O., Parra, J. B., Ferrer, M. L., & del Monte, F. (2011). Deep eutectic solvents as both precursors and structure directing agents in the synthesis of nitrogen-doped hierarchical carbons highly suitable for CO_2 capture. *Energy & Environmental Science*, *4*(9), 3535-3544. https://doi.org/10.1039/c1ee01463c.
41. Cao, T. P., Hang, C. N., Vu-Quang, H., Kabtamu, D. M., Kumar, S., Nguyen, V. C., & Cao, X. T. (2022). Catalyst-free synthesis of poly(furfuryl alcohol) using deep eutectic solvents. *New Journal of Chemistry = Nouveau Journal de Chimie*, *46*(8), 3786-3793. https://doi.org/10.1039/D1NJ05723E.
42. Tan, W. X., Chiang, P.-J., Tan, L. P., Ramanujan, R. V., Tan, M. J., Ong, A., Jangam, J. S. D., & Lai, C. Q. (2024). Adhesive and alloying properties of dual purpose polyfurfuryl alcohol binder for binder jet additive manufacturing of steel. *Additive Manufacturing*, *86*, 104212. https://doi.org/10.1016/j.addma.2024.104212.
43. Acosta, A. P., Amico, S. C., Delucis, R. A., Missio, A. L., Rodrigues, M. B. B., Ribeiro, A. C. R., Goularte, M. P., & Gatto, D. A. (2024). Surface analysis of different wood polymer composites exposed to artificial weathering. *Journal of Wood Chemistry and Technology*, *44*(2), 88-101. https://doi.org/10.1080/02773813.2023.2299814.

Received: Dec. 04, 2025
Revised: May 24, 2026
Accepted: May 28, 2026

Associate Editor: César L. Petzhold

Supplementary Material

Supplementary material accompanies this paper.

Table S1. WCAs of different modified sponge materials and their surface modification strategies reported in the literature.

This material is available as part of the online article from https://doi.org/10.1590/0104-1428.20250105